2021 IEEE/RSJ International Conference on Intelligent Robots and Systems (IROS)
September 27 - October 1, 2021. Prague, Czech Republic

Open-Loop Magnetic Actuation of Helical Robots using Position-Constrained Rotating Dipole Field

Ritwik Avaneesh, Roberto Venezian, Chang-Sei Kim, Jong-Oh Park, Sarthak Misra, and Islam S. M. Khalil

***Abstract*— Control of tetherless magnetically actuated helical robots using rotating dipole fields has a wide variety of medical applications. The most promising technique in manipulation of these robots involves a rotating permanent magnet controlled by a robotic manipulator. In this work, we study the open-loop response of helical robots (in viscous fluids characterized by low Reynolds numbers) in the presence of position constraints on the actuating rotating permanent magnet. We first derive a mapping between the space of the manipulator's joints, the produced magnetic fields in three-dimensional space, and the translational and rotational velocities of the helical robot. Then, we constrain the 3D position of the rotating dipole field and predict the response of the helical robot by controlling its angular velocity using the constrained mapping. We demonstrate open-loop control and gravity compensation of the robot using the angular velocities of the actuating permanent magnet while enforcing constraints on the end-effector position.**

I. INTRODUCTION

Over the past decade, robots at the nano- and micro-scales have shown potential to revolutionize medicine by reaching regions inaccessible to catheterization [1]–[4]. The locomotion of these tetherless devices capitalizes on the conversion of several forms of energies into mechanical energy or movement. Magnetic [5], [6], acoustic [7], chemical [8], electric [9], thermal [10], and light [11] energy have been utilized to actuate structures fabricated specifically to work upon sensing one, or a combination [12], of these external stimuli. Once the relation between the external energy and the behavior of the stimuli-responsive material in the fabricated structures is understood, a locomotion strategy is designed to work based on the environment and the potential application. For example, rolling or tumbling on a solid boundary [13], [14], swimming using the drag-based thrust [15], and pulling with a force [16] have been proven to be efficient locomotion strategies. The form of energy and the locomotion strategy must be selected specifically based on the physical surroundings, intended application, and the localization strategy. In practice, magnetic actuation using the drag-based thrust of helical microrobots is efficient under a wide range of Reynolds numbers (*Re*). In this case, it is reasonable to power these microrobots using actuating time-varying magnetic field produced by rotating permanent magnets fixed to the end-effector of a manipulator [17], as shown in Fig. 1. Scalability and adaptability are two direct consequences of the fact that the displacement of the actuating permanent magnet can be fully controlled in three-dimensional (3-D) space. First, the size of the workspace is no longer limited by the projection distance of the magnetic field, but rather depends on the relatively large workspace of the manipulator. Second, the configuration of this permanent magnet-based robotic system can be adapted to incorporate important functionalities like non-invasive imaging systems [18].

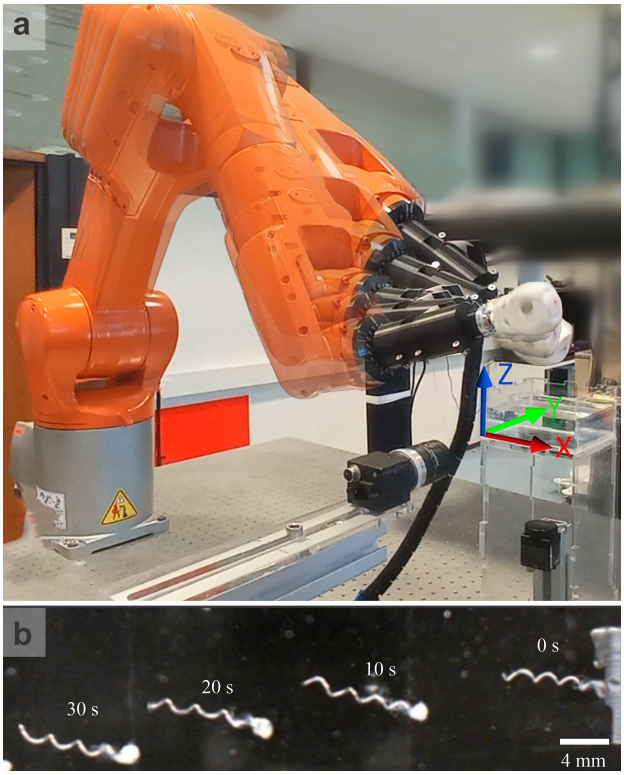

Fig. 1: Helical propulsion in viscous fluid is achieved using rotating magnetic fields. (a) An actuating rotating permanent magnet is controlled in three-dimensional (3-D) space by a six degree-of-freedom robotic manipulator. (b) The produced time-varying magnetic field drives a helical robot controllably inside a viscous fluid. The helical robot is controlled while enforcing a position constraint on actuating dipole field.

It has been shown that when a magnetic dipole, is rotated around a fixed axis such that the dipole is perpendicular to

R. Avaneesh, R. Venezian, S. Misra, and I. S. M. Khalil are with the Surgical Robotics Laboratory, Department of Biomechanical Engineering, Faculty of Engineering Technology, University of Twente, Enschede 7500 AE, The Netherlands.

C-S. Kim and J-O. Park are with the School of Mechanical Engineering, Chonnam National University, Gwangju 61186, Republic of Korea.

J-O. Park is also affiliated with the Korea Institute of Medical Microrobotics, Gwangju, 61011, Republic of Korea.

S. Misra is with the Department of Biomedical Engineering, University of Groningen and University Medical Center Groningen, Groningen 9713 GZ, The Netherlands.

This work is supported by a grant from the Korea Health Technology Development R&D Project through the Korea Health Industry Development Institute, funded by the Ministry of Health & Welfare, Republic of Korea under Grant HI19C0642.

the axis of rotation, the magnetic field vector at every point in space also rotates around a fixed axis [17]. Mahoney *et al.* have reformulated this phenomenon using linear algebraic techniques, which enables finding the necessary dipole rotation axis that is required to make the magnetic field at any desired point in space rotate about any desired axis [17]. Such method has been tested using a rotating permanent magnet fixed in space by a robotic manipulator to control the displacement of the magnet, and actuation of capsule endoscopes, helical swimmers, and spherical agents have been demonstrated inside fluid-filled confined environments. They have also demonstrated closed-loop control of three degree-of-freedom (3-DOF) and 2-DOF open-loop directional control of a magnetic capsule endoscope based on position feedback only [19]. These control results are implemented in the absence of constraints on the displacement of the actuating dipole field or the robotic manipulator.

In this paper, we control the motion of helical robots inside a viscous fluid in 3-D space using a rotating magnetic field produced by an actuating permanent magnet fixed to a robotic manipulator. We demonstrate the ability of the system to control the motion of the helical robot in the presence of a position constraint on the end-effector. We focus on changing the actuation axis of the rotating dipole field while keeping the magnet position fixed over time to follow a prescribed path whilst compensating for gravity in an open-loop way.

II. Modeling of Helical Propulsion and Magnetic Actuation

In low-Re, the response of the robot to an externally applied magnetic field is governed by balance between magnetic, viscous drag, and gravitational forces and torques.

A. Helical Propulsion in Low-Re

Suppose we consider a helical body with length L and magnetic moment $\mathbf{m}$ perpendicular to its helix axis, immersed in a viscous fluid, with density ρ_{f}, characterized by low-Re and actuated using non-uniform magnetic field, $\mathbf{B}$, as shown in Fig. 2. In low-Re, inertial forces are negligible and the motion of helical robot is governed by

$$\begin{aligned} \mathbf{f}_{\mathrm{visc}} + \mathbf{f}_{\mathrm{mag}} + \mathbf{f}_{\mathrm{g}} &= 0 \quad (1) \\ \mathbf{T}_{\mathrm{visc}} + \mathbf{T}_{\mathrm{mag}} + \mathbf{T}_{\mathrm{g}} &= 0, \quad (2) \end{aligned}$$

where $\mathbf{f}_{\mathrm{visc}}$ and $\mathbf{T}_{\mathrm{visc}}$ are the viscous drag force and torque, respectively. Further, $\mathbf{f}_{\mathrm{mag}}$ and $\mathbf{T}_{\mathrm{mag}}$ are the magnetic force and torque, respectively. Furthermore, $\mathbf{f}_{\mathrm{g}}$ and $\mathbf{T}_{\mathrm{g}}$ are the force and torque due to gravity, respectively. One direct consequence of the negligible inertia force is that the hydrodynamics is linear. Therefore, the viscous drag force and torque are given by

$$\begin{pmatrix} \mathbf{f}_{\mathrm{visc}} \\ \mathbf{T}_{\mathrm{visc}} \end{pmatrix} = \begin{pmatrix} \boldsymbol{A} & \boldsymbol{B} \\ \boldsymbol{B}^{\mathrm{T}} & \boldsymbol{C} \end{pmatrix} \begin{pmatrix} \mathbf{U} \\ \boldsymbol{\omega} \end{pmatrix}, \quad (3)$$

where $\mathbf{U}$ and $\boldsymbol{\omega}$ are the translational and angular velocity of the helical body due to the external force and torque, respectively. In Equation (3) the sub-matrices $\boldsymbol{A}$, $\boldsymbol{B}$, and $\boldsymbol{C}$ are calculated using the Resistive-Force Theory and are only dependent on the viscosity, η, of the medium and the geometry of the helical body [15]. In Equations (1)-(2), the magnetic force, $\mathbf{f}_{\mathrm{mag}}(\boldsymbol{p})$, and torque, $\mathbf{T}_{\mathrm{mag}}(\boldsymbol{p})$ at point, $\boldsymbol{p}$, are given by

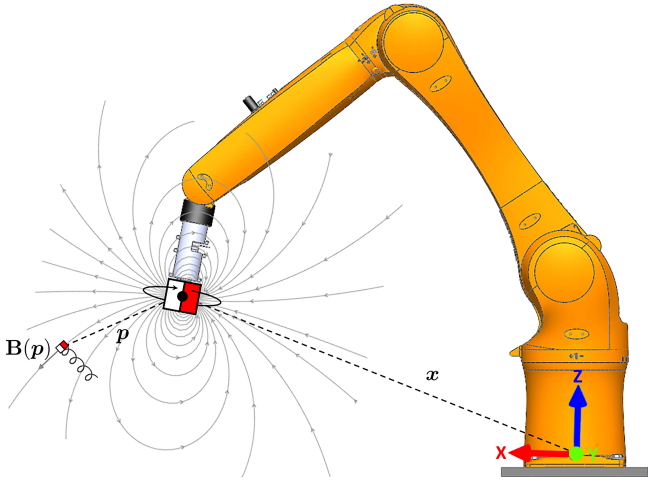

Fig. 2: A rotating actuating magnetic field, $\mathbf{B}(\boldsymbol{p})$, is produced by a permanent magnet. The displacement of the permanent magnet is controlled by a robotic manipulator. A helical robot with magnetic moment perpendicular to its long axis aligns along the rotating field lines and achieve helical propulsion in viscous fluid.

$$\begin{aligned} \mathbf{f}_{\mathrm{mag}}(\boldsymbol{p}) &= (\mathbf{m} \cdot \nabla)\mathbf{B}(\boldsymbol{p}) \quad (4) \\ \mathbf{T}_{\mathrm{mag}}(\boldsymbol{p}) &= \mathbf{m} \times \mathbf{B}(\boldsymbol{p}). \quad (5) \end{aligned}$$

Finally, in Equations (1)-(2) the force, $\mathbf{f}_{\mathrm{g}}$, and torque, $\mathbf{T}_{\mathrm{g}}$, exerted on the helical robot due to gravity are given by

$$\begin{aligned} \mathbf{f}_{\mathrm{g}} &= V(\rho_{\mathrm{r}} - \rho_{\mathrm{f}})\mathbf{g} \quad (6) \\ \mathbf{T}_{\mathrm{g}} &= (\mathbf{r}_{\mathrm{cov}} - \mathbf{r}_{\mathrm{com}}) \times \mathbf{f}_{\mathrm{g}}, \quad (7) \end{aligned}$$

where V is the volume the robot, ρ_{r} and ρ_{f} are its density and the density of the fluid, respectively. Furthermore, $\mathbf{g}$ signifies gravity, $\mathbf{r}_{\mathrm{cov}}$ and $\mathbf{r}_{\mathrm{com}}$ are the position vectors of the center of volume and center of mass, respectively. These force and torque complete the relation between the external forces and torques and the resulting velocities $\mathbf{U}$ and $\boldsymbol{\omega}$ of the robot.

B. Rotating Actuating Magnetic Fields

Equations (1)-(3) show the velocities of the helical robots can be directly determined from the balance between magnetic force, force due to gravity, and viscous drag. The magnetic force and torque are directly affected by the actuating magnetic field, $\mathbf{B}(\boldsymbol{p})$, which is given by the following point-dipole approximation:

$$\mathbf{B}(\boldsymbol{p}) = \frac{\mu_0}{4\pi}\left(\frac{3\boldsymbol{p}\boldsymbol{p}^{\mathrm{T}}}{\|\boldsymbol{p}\|^5} - \frac{\mathbb{I}}{\|\boldsymbol{p}\|^3}\right)\mathbf{M}(\boldsymbol{q}), \quad (8)$$

where $\mu_0 = 4\pi \times 10^{-7}$ N.A^{-2} is the permeability of free space, $\mathbf{M} \in SO(3)$ is the dipole moment of the actuator magnet and $\mathbb{I} \in \mathbb{R}^{3\times3}$ is the identity matrix. Equation (8) gives the magnetic field at the position of the robot, $\boldsymbol{p}$, when the permanent magnet is fixed at $\boldsymbol{x} \in \mathbb{R}^3$. Note that the magnetic field at a point, $\boldsymbol{p}$, is controlled by the joints of the manipulator.

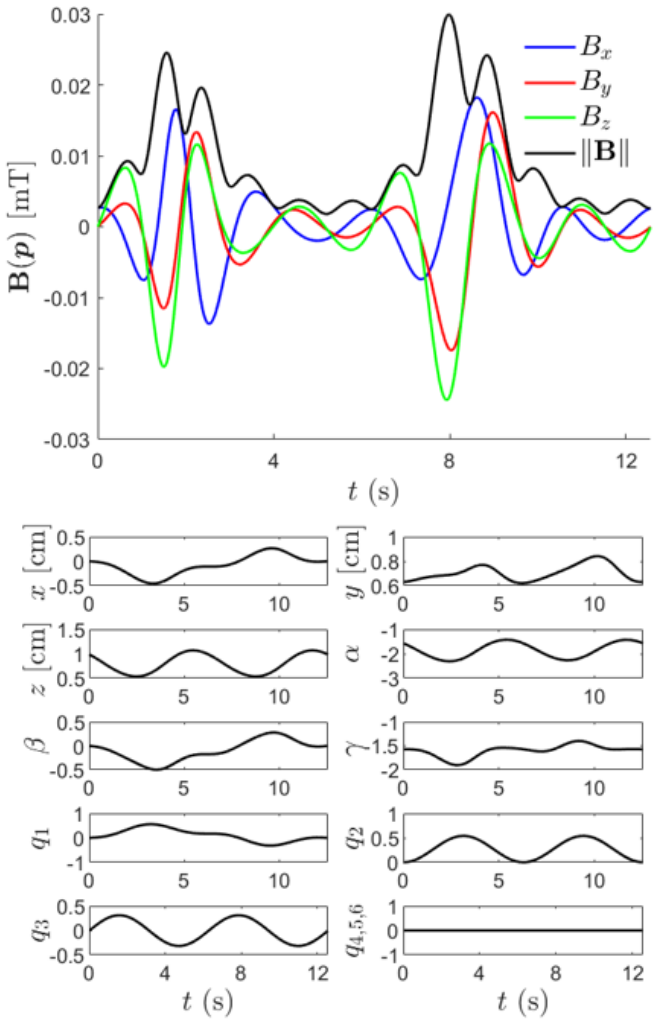

Fig. 3: The magnetic field at a point, $\boldsymbol{p}$, from the actuator magnet varies with the joint variables of the robotic manipulator $(q_1, \ldots, q_6)$. The coordinates x, y, and z characterize the position of the actuator magnet in the manipulator frame of reference, and the angles α, β, and γ characterize the orientation R.

The configuration-to-pose kinematics of the robotics manipulator is given by [20]

$$\{\boldsymbol{x}, R\} = \mathcal{F}(\boldsymbol{q}), \tag{9}$$

where $\mathcal{F} : \mathbb{R}^n \to \{\mathbb{R}^3, SO(3)\}$ is the forward kinematic mapping and $\boldsymbol{q} \in \mathbb{R}^n$ is the joint variables. Equations (8) and (9) provide the relation between the magnetic field at a point, $\boldsymbol{p}$, and the configuration of the robotic manipulator. Fig. 3 shows the magnetic field at a point calculated using Equation (8) and the corresponding position and orientation of the end-effector for a time-varying joint variables. It is convenient to represent the composed linear and angular velocities of the end-effector by the joint velocity, we have

$$\begin{pmatrix} \dot{\boldsymbol{x}} \\ \boldsymbol{\Omega} \end{pmatrix} = \mathbf{J}_{\mathrm{m}}(\boldsymbol{q})\dot{\boldsymbol{q}}, \tag{10}$$

where $\mathbf{J}_{\mathrm{m}} \in \mathbb{R}^{n \times n}$ is the manipulator Jacobian.

Mahoney and Abbott have shown that the velocity level kinematics (10) can also be modified to include the contribution of the magnetic moment of the actuator magnet using $\dot{\mathbf{M}} = \Omega \times \mathbf{M}$, and we obtain [19]

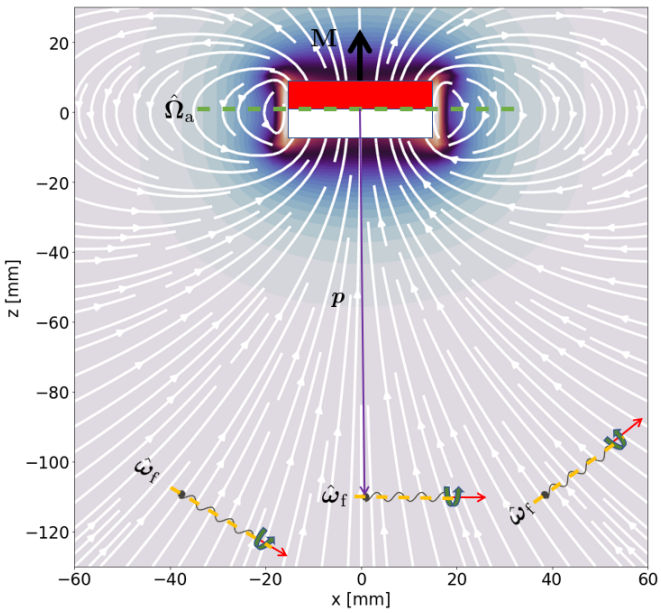

Fig. 4: Magnetic field lines generated by a permanent magnet with magnetization $\mathbf{M} = 18.89$ A.m^2 and $\|\mathbf{B}(\boldsymbol{p})\| = 2.75$ mT at $\boldsymbol{p} = \begin{bmatrix} 0 & 0 & -110 \end{bmatrix}^{\mathrm{T}}$ mm. The magnetic dipole moment of the helical robot is aligned along the magnetic field rotation axis, $\hat{\boldsymbol{\omega}}_{\mathrm{f}}$. Control of the axis of rotation of the actuator magnet, $\hat{\boldsymbol{\Omega}}_{\mathrm{a}}$, enables the robot to swim controllably and compensate its own weight.

$$\begin{pmatrix} \dot{\boldsymbol{x}} \\ \dot{\mathbf{M}} \end{pmatrix} = \begin{pmatrix} \mathbb{I} & 0 \\ 0 & \mathrm{SK}(\mathbf{M}) \end{pmatrix} \mathbf{J}_{\mathrm{m}}(\boldsymbol{q})\dot{\boldsymbol{q}} = \mathbf{J}_{\mathrm{A}}(\boldsymbol{q})\dot{\boldsymbol{q}}, \tag{11}$$

where $\mathrm{SK}(\cdot) : \mathbb{R}^3 \to SO(3)$ is the skew-symmetric operator of the cross product and $\mathbf{J}_{\mathrm{A}} \in \mathbb{R}^{n \times n}$ is the actuator permanent magnet Jacobian. Equation (11) completes the relation between the joint velocities of the manipulator and the helical robot velocity, composed by the linear velocity $\mathbf{U}$ and the angular velocity $\boldsymbol{\omega}$.

C. Actuation using Pose-Constrained Dipole Field

To test the helical propulsion under a position constraint on the actuator magnet, we shall invoke $\dot{\boldsymbol{x}} = 0$ into Equation (12), which yields

$$\begin{pmatrix} 0 \\ \dot{\mathbf{M}} \end{pmatrix} = \begin{pmatrix} \mathbf{J}_{\mathrm{m}}^{11}(\boldsymbol{q}) & \mathbf{J}_{\mathrm{m}}^{12}(\boldsymbol{q}) \\ \mathrm{SK}(\mathbf{M})\mathbf{J}_{\mathrm{m}}^{21}(\boldsymbol{q}) & \mathrm{SK}(\mathbf{M})\mathbf{J}_{\mathrm{m}}^{22}(\boldsymbol{q}) \end{pmatrix} \dot{\boldsymbol{q}}, \tag{12}$$

where $\mathbf{J}_{\mathrm{m}}^{11}(\boldsymbol{q})$, $\mathbf{J}_{\mathrm{m}}^{12}(\boldsymbol{q})$, $\mathbf{J}_{\mathrm{m}}^{21}(\boldsymbol{q})$, and $\mathbf{J}_{\mathrm{m}}^{22}(\boldsymbol{q})$ are the submatrices of the geometric Jacobian. Equations (12) maps the joint velocities into angular velocity of the actuator magnet without translation. If the translation and rotation of the actuator magnet are kept constant (Fig. 4), then the helical robot will ultimately align along the the magnetic field $\mathbf{B}(\boldsymbol{p})$. In this case, the magnetic field rotation axis, $\hat{\boldsymbol{\omega}}_{\mathrm{f}}$, and the actuator magnet's rotation axis, $\hat{\boldsymbol{\Omega}}_{\mathrm{a}}$, are given as $\hat{\boldsymbol{\Omega}}_{\mathrm{a}} = \widehat{\mathbf{H}\hat{\boldsymbol{\omega}}_{\mathrm{f}}}$, where $\mathbf{H} = 3\hat{\boldsymbol{p}}\hat{\boldsymbol{p}}^{\mathrm{T}} - \mathbb{I}$. Therefore, the rotation axis of the magnetic field varies with the position of the helical robot with respect to the actuator magnet, $\boldsymbol{p}$, and it is not possible to maintain the swimming direction along a straight line (along the $\mathbf{x}$-axis). The angular velocity of the

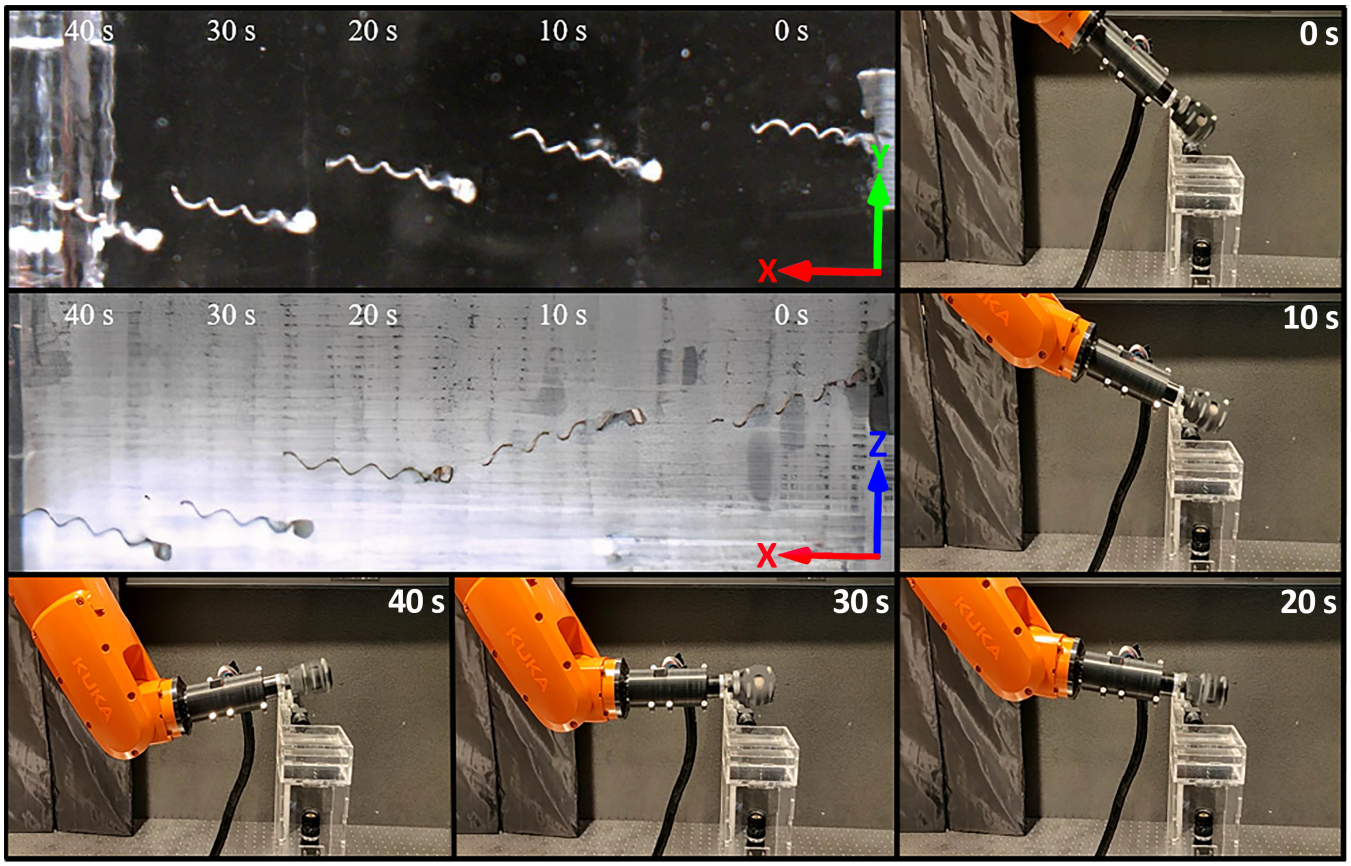

Fig. 5: Motion control achieves helical propulsion in the presence of a constraint on the position of the actuating permanent magnet. The robot swims controllably under the influence of a rotating magnetic field at actuation frequency of 5 Hz. The robot swims at a maximum velocity of $U = 1.43$ mm/s in silicon oil with density $\rho_f = 971$ kg/m^3 and viscosity of $\eta = 1$ Pa.s ($Re = 10^{-2}$).

actuator magnet must be controlled using Equation (12) to orient the rotation axis of the magnetic field parallel to the $\mathbf{x}$-axis and enable forward swimming.

III. Experimental Results

Open-loop motion control experiments are conducted using the permanent magnet-based robotic system shown in Fig. 1 to drive the robot along a prescribed path while enforcing a constraint on the end-effector, as shown in Fig. 5.

A. System Description

Our system consists of a 6-DOF serial manipulator (KUKA KR-1100-2, KUKA, Augsburg, Germany) to control the displacement of the rotating disc permanent magnet. The magnet (NdFeB Grade-N45) has a diameter of 35 mm, height of 20 mm, and is axially magnetized. The magnetic flux density of the actuator magnet is measured using a SENIS 3-axis digital Teslameter at varying distance, $\boldsymbol{p}$. The magnitude of the dipole moment $\|\mathbf{M}\|$ is determined using a least squares solution for the point-dipole model. In this experiment, 50 samples of the flux density are measured between 40 mm and 100 mm from the center of the magnet, resulting in $\|\mathbf{M}\| = 18.89$ A.m^2.

The disc magnet is actuated by a Maxon 18V brushless DC motor with Hall-effect sensors, encoder and a planetary gearbox with gear ratio of 3.7:1. The motor is controlled using an EPOS4 Compact 50/5 CAN, digital position controller. The continuous rotation of the permanent magnet enables the robot to achieve helical propulsion. The kinematics and the Denavit-Hartenberg parameters from the base frame to the end-effector and to the actuator magnet frames of reference are provided in Appendix A.

The robot consists of a cylindrical permanent magnet (NdFeB Grade-N52) with diameter of 1 mm and height of 1 mm, attached to a helical body such that the helix axis is perpendicular to the dipole moment. The helix has length, pitch and radius of 11.7 mm, 3 mm and 0.6 mm, respectively. The robot is immersed in silicon oil (reservoir of dimensions 100 mm $\times$ 100 mm $\times$ 50 mm) with density of $\rho_f = 970$ kg/m^3 and viscosity of $\eta = 1$ Pa.s. Motion of the robot is measured using two FLIR Blackfly cameras in the $\mathbf{x}$-$\mathbf{y}$ and $\mathbf{x}$-$\mathbf{z}$ plane. Both cameras are fitted with Fujinon lens of 6 mm fixed focal length producing sub-millimeter tracking accuracy at 60 frames per second.

The entire system is programmed and modeled through Matlab Interface (Version R2020a). To achieve real-time control of the the robotic manipulator, a connection between RoboDK (RoboDK Inc., Montreal, Canada) and the robotic manipulator was established to move it automatically using RoboDK's user interface. The connection was established through a standard Ethernet connection (TCP/IP). For this purpose, a KUKAVARPROXY (Imts Srl, Taranto, Italy) server was installed on the KRC4 controller (KUKA,

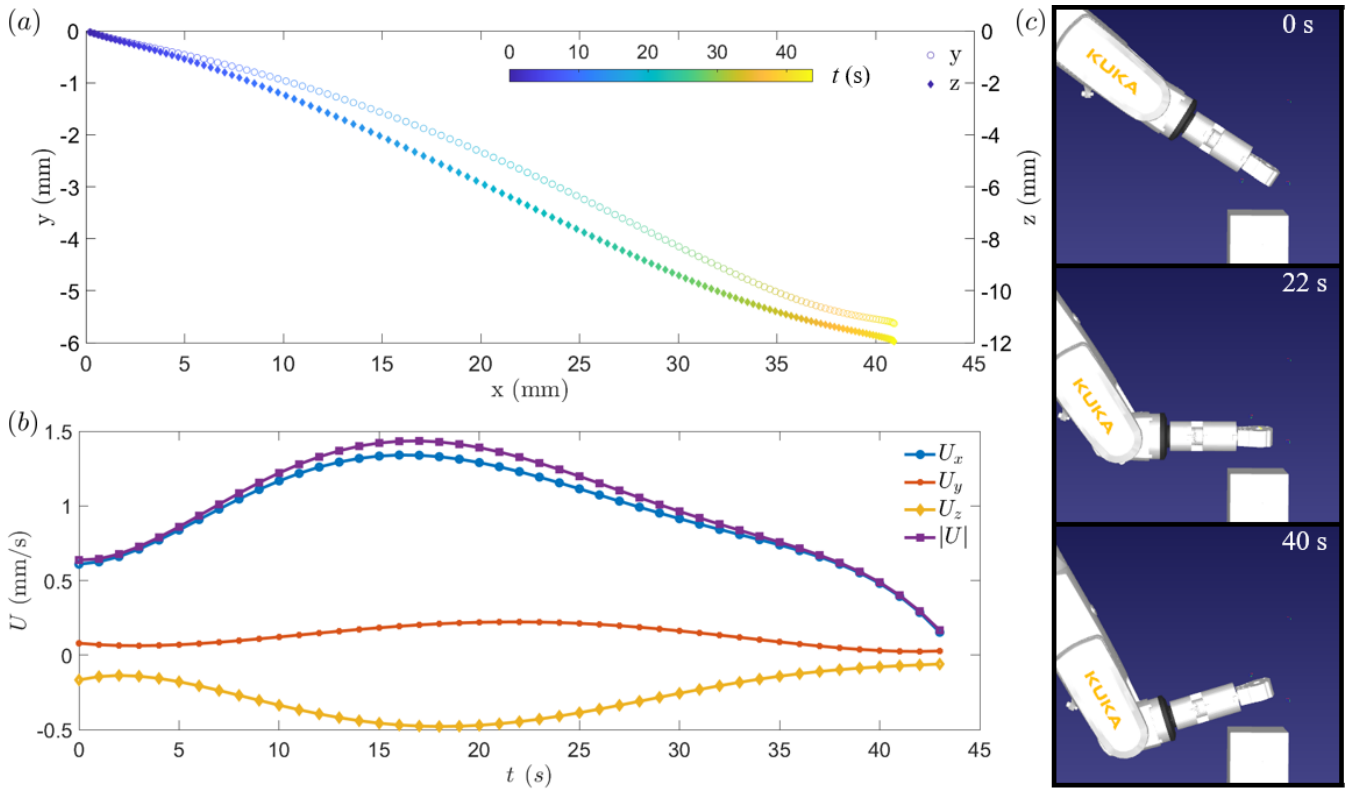

Fig. 6: Experimental motion control result demonstrates swimming under the influence of a rotating field produced by a constrained actuating magnet. The robot swims in silicone oil ($\rho_f = 971$ kg/m^3 and $\eta = 1$ Pa.s) at an average speed of $U = 0.98$ mm/s and has Reynolds number of $Re = 10^{-3}$. Maximum swimming speed is achieved at $t = 17$ seconds when the robot swims toward the permanent magnet and the magnetic force contributes to its propulsive thrust.

Augsburg, Germany) of the robotic manipulator. This server allows the global variables from the robotic arm controller to be exchanged with the remote RoboDK's user interface.

B. Open-Loop Control of the Helical Robot

To control the helical robot along a desired path it is critical to select the appropriate rotation axis $\hat{\boldsymbol{\omega}}_f$ of the magnetic field. When the robot swims away from the nearby solid boundary and in the absence of any interactions, its rotation axis aligns with $\hat{\boldsymbol{\omega}}_f$. Therefore, it is convenient to steer the helical robot by controlling $\hat{\boldsymbol{\Omega}}_a$. In addition, the rotation axis of the magnetic actuator can be determined using the prescribed trajectory of the desired path such that $\hat{\boldsymbol{\omega}}_f$ and the local tangent are perpendicular.

Fig. 5 shows a representative open-loop control result of the helical robot along a straight line along the $\mathbf{x}$-axis. Therefore, the rotation axis of the magnetic field, $\hat{\boldsymbol{\omega}}_f$, is made parallel to the $\mathbf{x}$-axis, while the constraint on the position of the actuating permanent magnet is enforced using Equations (12). In this experiment, the robot swims at a maximum swimming speed of $U = 1.43$ mm/s at actuation frequency of 5 Hz. The step-out frequency of the robot is 12 Hz. Therefore, the swimming speed of the robot can be controlled by increasing the actuation frequency of the magnetic field below the step-out frequency. In this case, the angular velocity of the rotating dipole field will depend on the linear velocity of the robot based on Equations (1)-(8).

The swimming path of the helical robot is shown in the $\mathbf{x}$-$\mathbf{y}$ and $\mathbf{x}$-$\mathbf{z}$ planes. This experimental result shows that associated with the translational motion of the helical robot is a continuous change in the angular velocity of the actuator magnet, as shown using the representative configurations of the robotic manipulator at $t = 0$, $t = 22$, and $t = 40$ seconds. The helical robot swims at an average velocity of 0.98 mm/s along the $\mathbf{x}$-axis and 0.15 mm/s along the $\mathbf{y}$-axis, as shown in Fig. 6. The average speed of the robot along the $\mathbf{z}$-axis is 0.3 mm/s. For $0 < t \leq 20$ seconds, the forward swimming speed of the robots increases as the distance to the actuator magnet decreases. At $t > 20$ seconds, the swimming speed decreases at the same rate as the gap with the actuator magnet increases. The positive and negative slopes of the forward swimming velocity signifies that the magnetic force (4) plays an important role and contributes to the net propulsive thrust of the robot. At $t = 22$ seconds, the robot is radially-actuated as the axis of the actuating magnet and the long axis of the robot are aligned. As the robot moves away from the actuator magnet, the magnetic force acts against the propulsive trust and we observe a noticeable decrease in the swimming speed, as shown in Fig. 6.

IV. Conclusions and Future Work

Magnetic actuation of helical robots is achieved using a rotating dipole field in the presence of a constraint on its position. We derive the mapping between the robot velocity, composed by linear and angular velocity, and the joint velocities of the robotic manipulator which fix the constrained

rotating permanent magnet. The helical robot is actuated in a viscous fluid characterized by low-Re using rotating magnetic fields produced by a permanent magnet fixed in space by the robotic manipulator. Our experimental results demonstrate the capability to actuate the robot controllably and compensate for its gravity by controlling the angular velocities of the constrained actuator magnet.

As part of future work, we will implement closed-loop control of the helical robot in 3-D space in the presence of position constraint on the actuator magnet. In addition, we will modify our permanent magnet-based robotic system to actuate the helical robots using two synchronized rotating dipole fields [22]. In the current study, we have demonstrated radial actuation and gravity compensation by the pulling magnetic force of the actuator magnet. To achieve closed-loop motion control in 3-D space, we will mitigate the pulling magnetic forces along the lateral directions of the robots using two synchronized actuating magnets.

REFERENCES

[1] J. Wang and W. Gao, "Nano/Microscale motors: biomedical opportunities and challenges," *ACS Nano*, vol. 6, no. 7, pp. 5745-5751, 2012.

[2] B. J. Nelson, I. K. Kaliakatsos, and J. J. Abbott, "Microrobots for minimally invasive medicine," *Annual Review of Biomedical Engineering*, vol. 12, pp. 55-85, 2010.

[3] A. Hosney, J. Abdalla, I. S. Amin, N. Hamdi, and I. S. M. Khalil, "*In vitro* validation of clearing clogged vessels using microrobots," in *Proceedings of the IEEE RAS/EMBS International Conference on Biomedical Robotics and Biomechatronics (BioRob)*, UTown, Singapore, pp. 272–277, 2016.

[4] M. Sitti, H. Ceylan, W. Hu, J. Giltinan, M. Turan, S. Yim, and E. Diller, "Biomedical applications of untethered mobile milli/microrobots," *Proceedings of the IEEE*, vol. 103, no. 2, pp. 205-224, 2015.

[5] K. E. Peyer, L. Zhang, and B. J. Nelson, "Bio-inspired magnetic swimming microrobots for biomedical applications," *Nanoscale*, vol. 5, no. 4, pp. 1259-1272, 2012.

[6] A. Ghosh and P. Fischer, "Controlled propulsion of artificial magnetic nanostructured propellers," *Nano Letters*, vol. 9, pp. 2243-2245, 2009.

[7] W. Wang, L. A. Castro, M. Hoyos, and T. E. Mallouk, "Autonomous motion of metallic microrods propelled by ultrasound," *ACS Nano*, vol. 6, no. 7, pp. 6122–6132, 2012.

[8] W. F. Paxton, K. C. Kistler, C. C. Olmeda, A. Sen, S. K. St. Angelo, Y. Cao, T. E. Mallouk, P. E. Lammert, and V. H. Crespi, "Catalytic nanomotors: autonomous movement of striped nanorods," *Journal of the American Chemical Society*, vol. 126, no. 41, pp. 13424–13431, 2004.

[9] P. Calvo-Marzal, S. Sattayasamitsathit, S. Balasubramanian, J. R. Windmiller, C. Dao, and J. Wang, "Propulsion of nanowire diodes," *Chemical Communications*, vol. 46, no. 10, pp. 1623–1624, 2010.

[10] J. Lapointe and S. Martel, "Thermoresponsive hydrogel with embedded magnetic nanoparticles for the implementation of shrinkable medical microrobots and for targeting and drug delivery applications," in *Proceedings of the Annual International Conference of the IEEE Engineering in Medicine and Biology Society*, pp. 4246–4249, 2009.

[11] S. Palagi, A. G. Mark, S. Y. Reigh, K. Melde, T. Qiu, H. Zeng, C. Parmeggiani, D. Martella, A. Sanchez-Castillo, N. Kapernaum, F. Giesselmann, D. S. Wiersma, E. Lauga, and P. Fischer, "Structured light enables biomimetic swimming and versatile locomotion of photoresponsive soft microrobots," *Nature Material*, vol. 15, pp. 647–653, 2016.

[12] J. Li, T. Li, T. Xu, M. Kiristi, W. Liu, Z. Wu, and J. Wang, "Magneto–Acoustic hybrid nanomotor," *Nano Letters*, vol. 15, pp. 4814–4821, 2015.

[13] A. W. Mahoney and J. J. Abbott, "Managing magnetic force applied to a magnetic device by a rotating dipole field," *Applied Physics Letters*, vol. 99, 2011.

[14] W. Jing, N. Pagano, and D. J. Cappelleri, "A tumbling magnetic microrobot with flexible operating modes," in *Proceedings of the IEEE International Conference on Robotics and Automation (ICRA)*, Karlsruhe, Germany, pp. 5514–5519, 2013.

[15] E. M. Purcell, "Life at low Reynolds number," *American Journal of Physics*, vol. 45, no. 1, pp. 3-11, 1977.

[16] M. P. Kummer, J. J. Abbott, B. E. Kratochvil, R. Borer, A. Sengul, and B. J. Nelson, "OctoMag: An Electromagnetic System for 5-DOF Wireless Micromanipulation," in IEEE Transactions on Robotics, vol. 26, no. 6, pp. 1006-1017, 2010.

[17] A. W. Mahoney, D. L. Cowan, K. M. Miller, and J. J. Abbott, "Control of untethered magnetically actuated tools using a rotating permanent magnet in any position," in *Proceedings of the IEEE International Conference on Robotics and Automation (ICRA)*, pp. 3375-3380, 2012.

[18] S. Tognarelli, V. Castelli, G. Ciuti, C. Di Natali, E. Sinibaldi, P. Dario, and A. Menciassi, "Magnetic propulsion and ultrasound tracking of endovascular devices," *Journal of Robotic Surgery*, vol. 6, no. 1, pp. 5–12, 2012.

[19] A. W. Mahoney and Jake J. Abbott, "Five-degree-of-freedom manipulation of an untethered magnetic device in fluid using a single permanent magnet with application in stomach capsule endoscopy," *the International Journal of Robotics Research*, vol. 35, no. 1-3, pp. 129–147, 2016.

[20] R. M. Murray, Z. Li, and S. S. Sastry (1994). A Mathematical Introduction to Robotic Manipulation, 1st edn, CRC Press Inc., Boca Raton, FL, USA.

[21] T. Xu, Y. Guan, J. Liu, and X. Wu, "Image-Based visual servoing of helical microswimmers for planar path following," *IEEE Transactions on Automation Science and Engineering*, vol. 17, no. 1, pp. 325–333, 2020.

[22] A. Hosney, A. Klingner, S. Misra, and I. S. M. Khalil, "Propulsion and steering of helical magnetic microrobots using two synchronized rotating dipole fields in three-dimensional space," in *Proceedings of the IEEE/RSJ International Conference on Intelligent Robots and Systems (IROS)*, Rome, Italy, pp. 1988-1993, 2012.

APPENDIX A: DENAVIT-HARTENBERG PARAMETERS OF THE ROBOTIC MANIPULATOR

The Denavit-Hartenberg parameters of the robotic manipulator are provided in Table I. The homogeneous transformation matrix, $\mathbf{T}_{\mathrm{b}}^{0}$, describes the transformation from the base frame of the robotic manipulator to the rotating permanent magnet that is attached to the end-effector. This magnet produces the required magnetic field, $\mathbf{B}$, at position $\boldsymbol{p}$ relative to the helical microrobot, such that

$$\mathbf{T}_{\mathrm{b}}^{0} = \mathbf{T}_{6}^{0}(\boldsymbol{q})\mathbf{T}_{\mathrm{M}}^{6}(\boldsymbol{q}_{\mathrm{M}})\mathbf{T}_{\mathrm{b}}^{\mathrm{M}}(\boldsymbol{r}, \mathbf{M}) \tag{13}$$

where $\mathbf{T}_{6}^{0}(\boldsymbol{q})$ is the homogeneous transformation matrix of the robotic manipulator from the joint space coordinates $\boldsymbol{q} = [\theta_1, \ldots, \theta_6]$ to the Cartesian coordinates of the end-effector. Further, $\mathbf{T}_{\mathrm{M}}^{6}$ is the transformation from the permanent magnet to the end-effector's position. Finally, the transformation $\mathbf{T}_{\mathrm{b}}^{\mathrm{M}}(\boldsymbol{r}, \mathbf{M})$ maps the distance $\boldsymbol{r}$ to a location $\boldsymbol{p}$ and magnetization vector $\mathbf{M}$ to the magnetic field in the desired location.

TABLE I: The Denavit-Hartenberg parameters of the manipulator are used in Equation (13) to determine $\mathbf{M}$ in the mapping (12).

q_i	θ	α	a [mm]	d [mm]	$\theta_{\min}$	$\theta_{\max}$
q_1	0°	0	0	400	-170°	170°
q_2	0°	-90°	25	0	-190°	45°
q_3	$\theta_3 - 90^\circ$	0	560	0	-120°	156°
q_4	θ_4	-90°	25	515	-185°	185°
q_5	θ_5	90°	0	0	-120°	120°
q_6	$\theta_6 + 180^\circ$	-90°	0	90	-350°	350°